Supplementary Material

Pressure-induced superconductivity in $Bi_{2-x}Sb_xTe_{3-y}Se_y$

Tong He[1], Xiaofan Yang[1], Tomoya Taguchi[1], Teppei Ueno[1], Kaya Kobayashi[1], Jun Akimitsu[1], Hitoshi Yamaoka[2], Hirofumi Ishii[3], Yen-Fa Liao[3], Hiromi Ota[4], Hidenori Goto[1], Ritsuko Eguchi[1], Kensei Terashima[1], Takayoshi Yokoya[1], Harald O. Jeschke[1], Xianxin Wu[5], Yoshihiro Kubozono[1*]

[1] Research Institute for Interdisciplinary Science, Okayama University, Okayama 700-8530, Japan
[2] RIKEN SPring-8 Center, Hyogo 679-5148, Japan
[3] National Synchrotron Radiation Research Center, Hsinchu 30076, Taiwan
[4] Advanced Science Research Center, Okayama University, Okayama 700-8530, Japan
[5] Institute for Theoretical Physics and Astrophysics, University of Würzburg, 97074 Würzburg, Germany

Details of Crystal Growth

Stoichiometric amounts of Bi, Sb, Te, and Se powders with purity of higher than 99.99%, in which total mass was 1 g, were mixed and pelletized, and the pellet sample was sealed in an evacuated quartz tube. It was heated at 850°C for a day, slowly cooled to 550°C at a rate of 6°C / h and heated at 550°C for 2days. The quartz tube was then immersed to water, *i.e.*, the sample was quenched to obtain single crystals with a clear surface reflecting the basal plane. For all $Bi_{2-x}Sb_xTe_{3-y}Se_y$ samples, the same way was employed to obtain the single crystals. All peaks of XRD pattern measured using CuKα source (λ=1.54059 Å) were indexed by Bi_2Se_3 structure (space group No. 166, $R\bar{3}$m), as shown in Figure S1 for x=1.0 and y=1.0 as example.

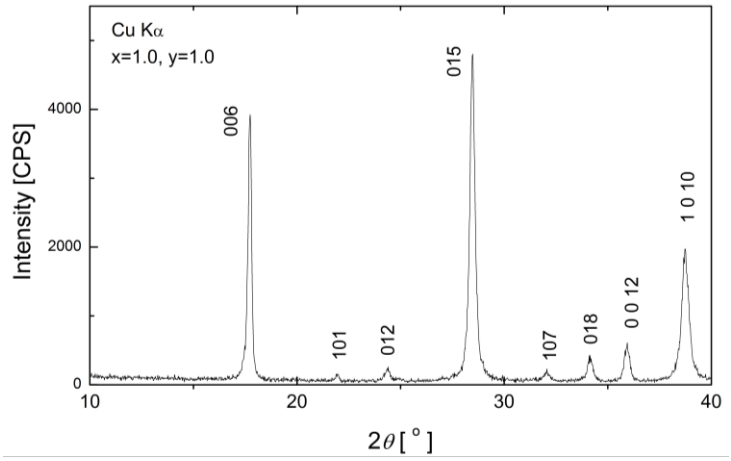

Figure S1. X-ray diffraction pattern on powder sample of $BiSbTe_2Se$. All the peaks are indexed by Bi_2Se_3 structure.

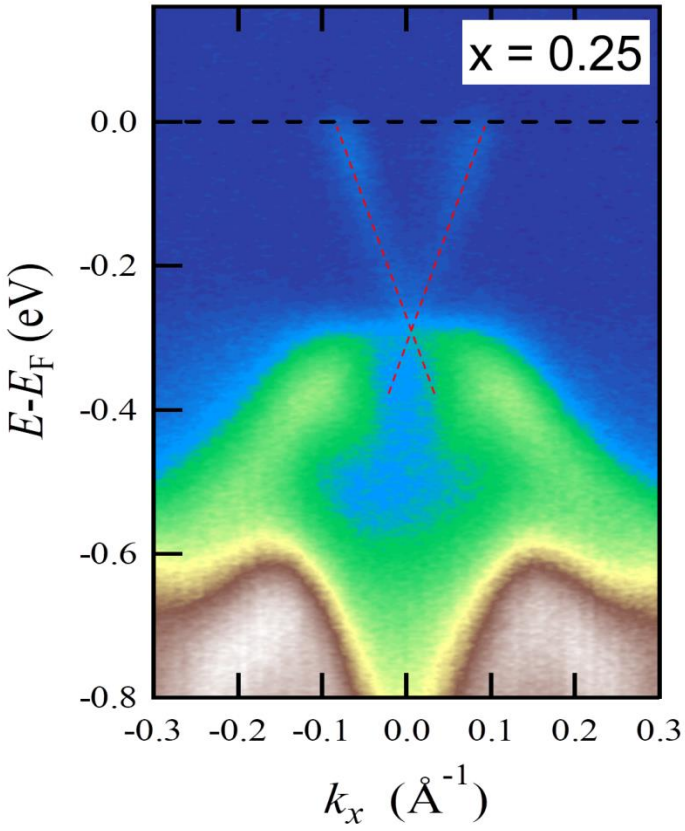

Figure S2. ARPES data of $Bi_{2-x}Sb_xTe_{3-y}Se_y$ (x = 0.25 and y = 1.0); the stoichiometry from EDX is '$Bi_{1.75(4)}Sb_{0.25(4)}Te_{1.89(7)}Se_{1.11(7)}$'.

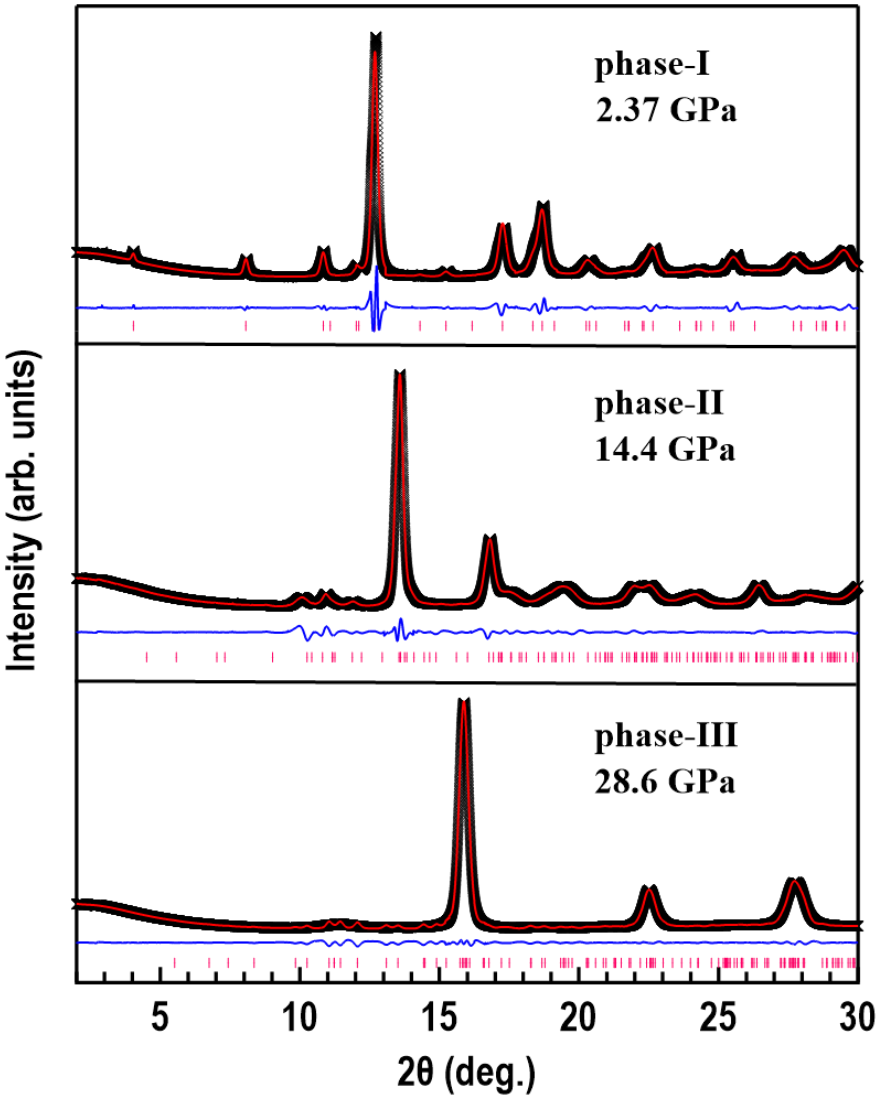

Figure S3. Experimental XRD patterns (black cross) of $Bi_{2.1(1)}Te_{1.8(2)}Se_{1.2(2)}$ at 2.37 GPa, 14.4 GPa, and 28.6 GPa, together with the patterns (red line) calculated by Le Bail fitting. The blue lines and pink ticks refer to the difference between experimental and calculated patterns, and positions of Bragg reflections predicted by lattice constants.

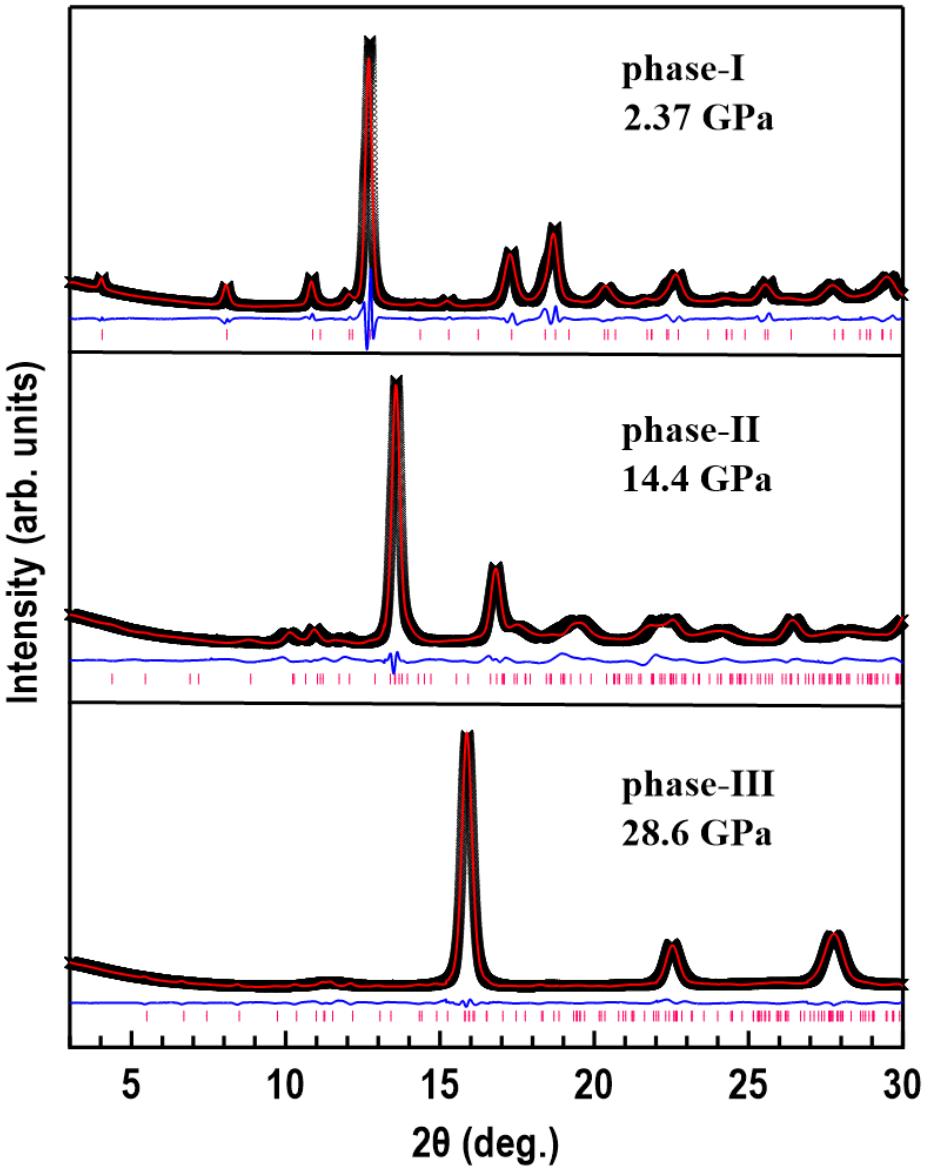

Figure S4. Experimental XRD patterns (black cross) of $Bi_{2.1(1)}Te_{1.8(2)}Se_{1.2(2)}$ at 2.37 GPa, 14.4 GPa and 28.6 GPa, together with the patterns (red line) calculated by Rietveld refinement. The blue lines and pink ticks refer to the difference between experimental and calculated patterns, and positions of Bragg reflections predicted by lattice constants and structural parameters.

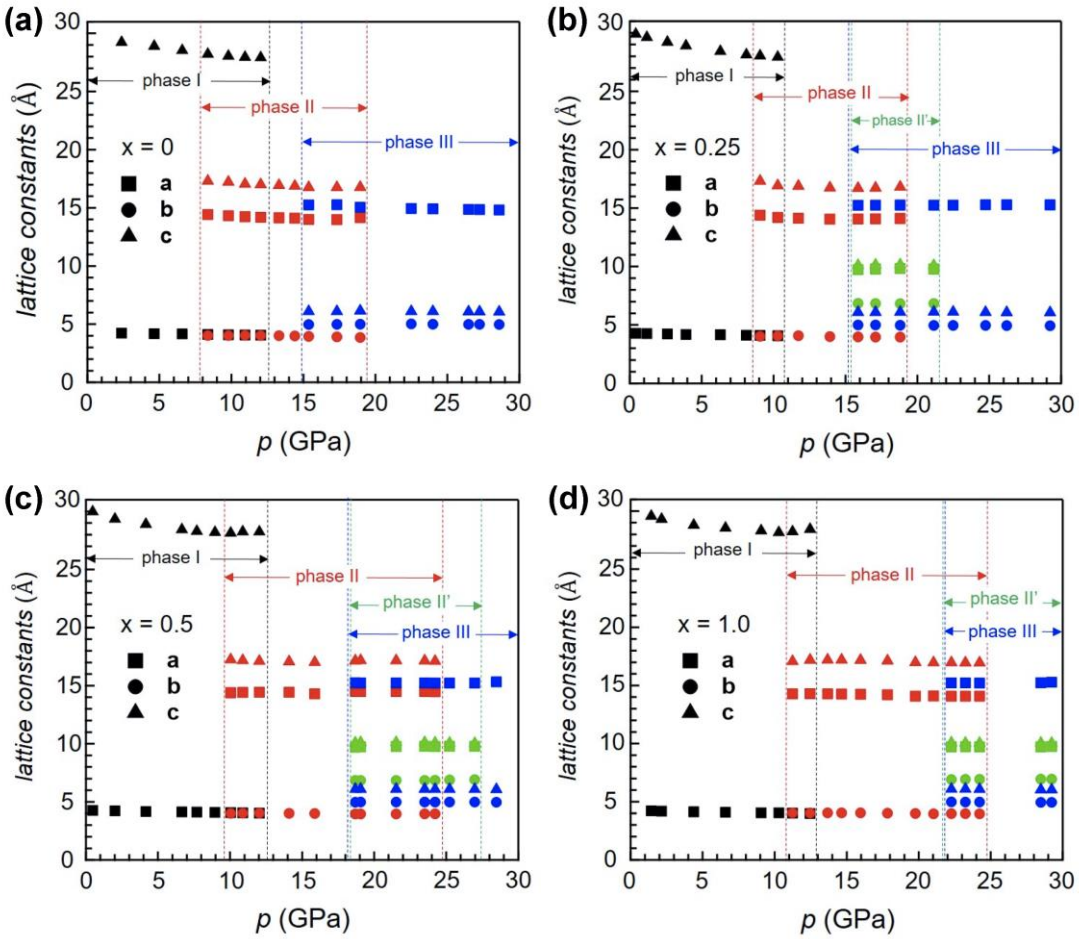

Figure S5. Plots of lattice constants against pressure for $Bi_{2-x}Sb_xTe_{3-y}Se_y$. Nominal x is shown in each graph; nominal y = 1. The stoichiometry determined from EDX is listed in Table 1.

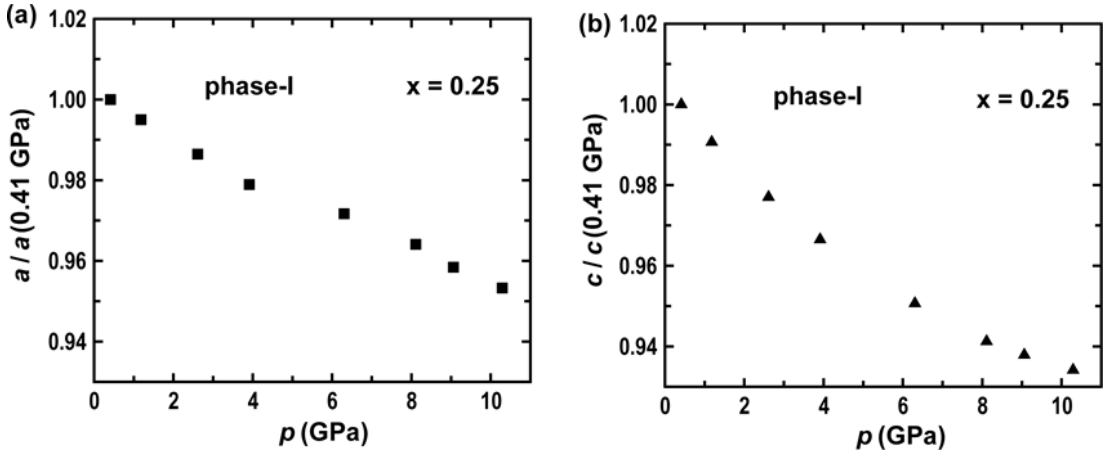

Figure S6. (a) *a* / *a*(0.41 GPa) and (b) *c* / *c*(0.41 GPa) as a function of pressure in phase-I of $Bi_{2-x}Sb_xTe_{3-y}Se_y$ (x = 0.25 and y = 1.0), $Bi_{1.75}Sb_{0.25}Te_2Se$.

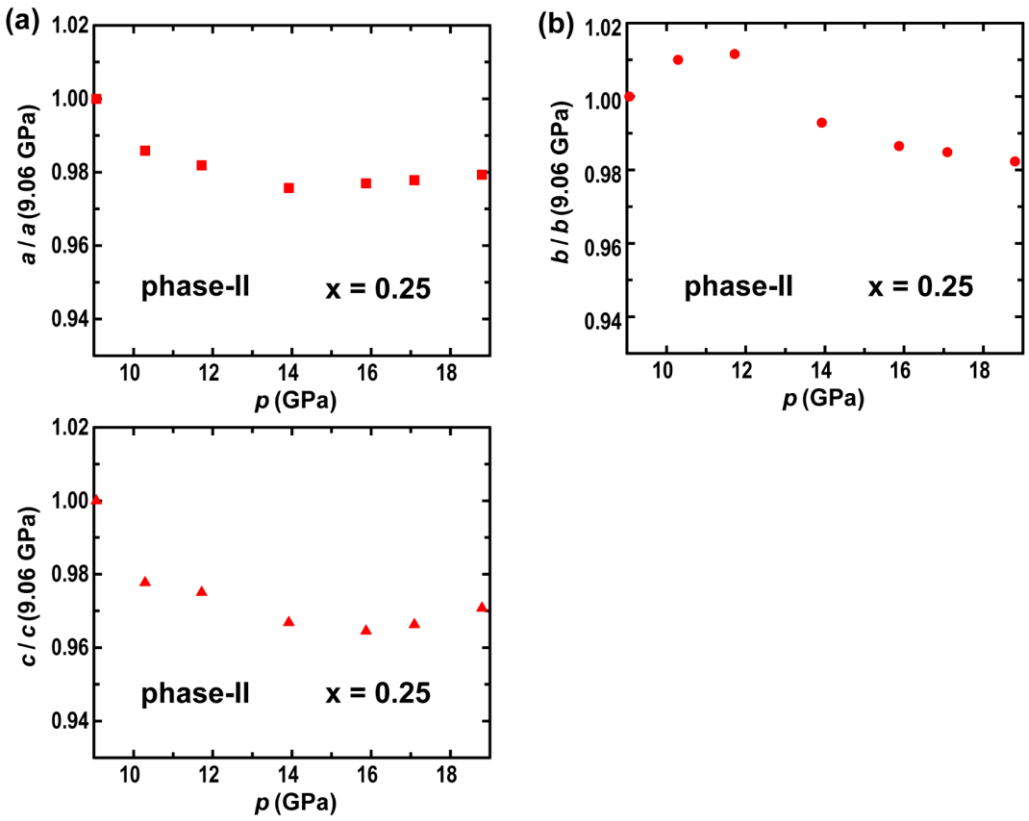

Figure S7. (a) *a* / *a*(9.06 GPa), *b* / *b*(9.06 GPa) and *c* / *c*(9.06 GPa) as a function of pressure in phase-II of $Bi_{2-x}Sb_xTe_{3-y}Se_y$ (x = 0.25 and y = 1.0), $Bi_{1.75}Sb_{0.25}Te_2Se$.

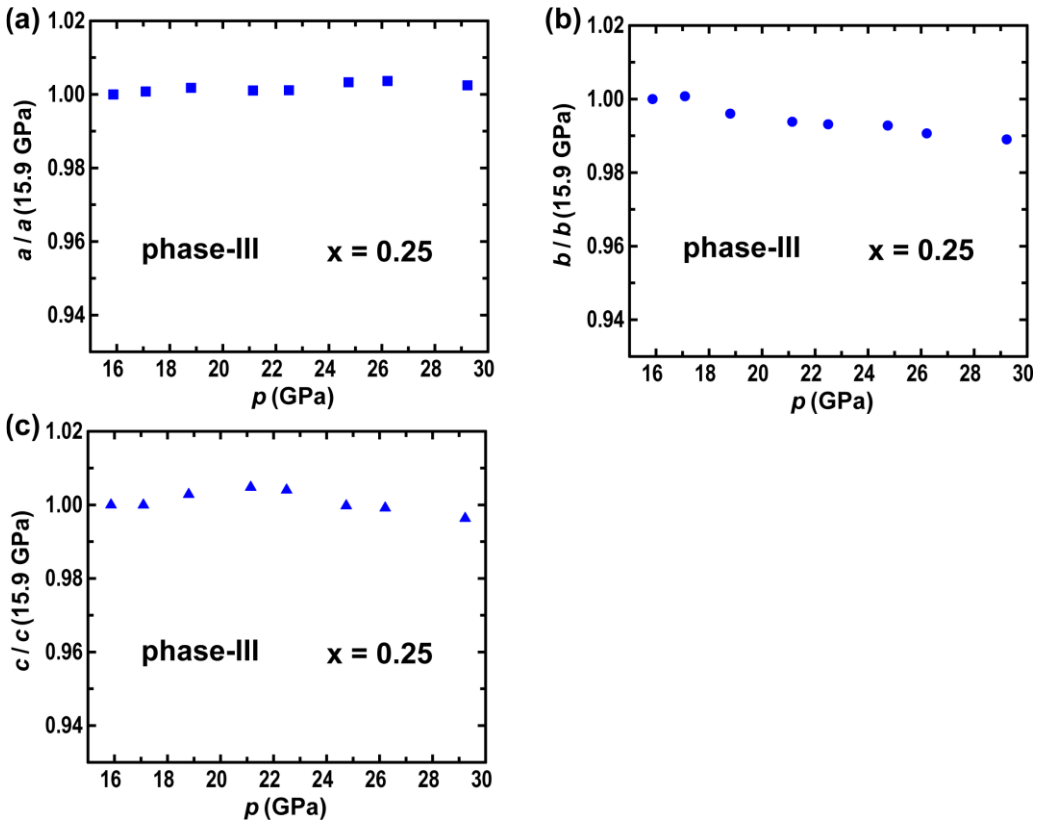

Figure S8. (a) *a* / *a*(15.9 GPa), *b* / *b*(15.9 GPa) and *c* / *c*(15.9 GPa) as a function of pressure in phase-II of $Bi_{2-x}Sb_xTe_{3-y}Se_y$ (x = 0.25 and y = 1.0), $Bi_{1.75}Sb_{0.25}Te_2Se$.

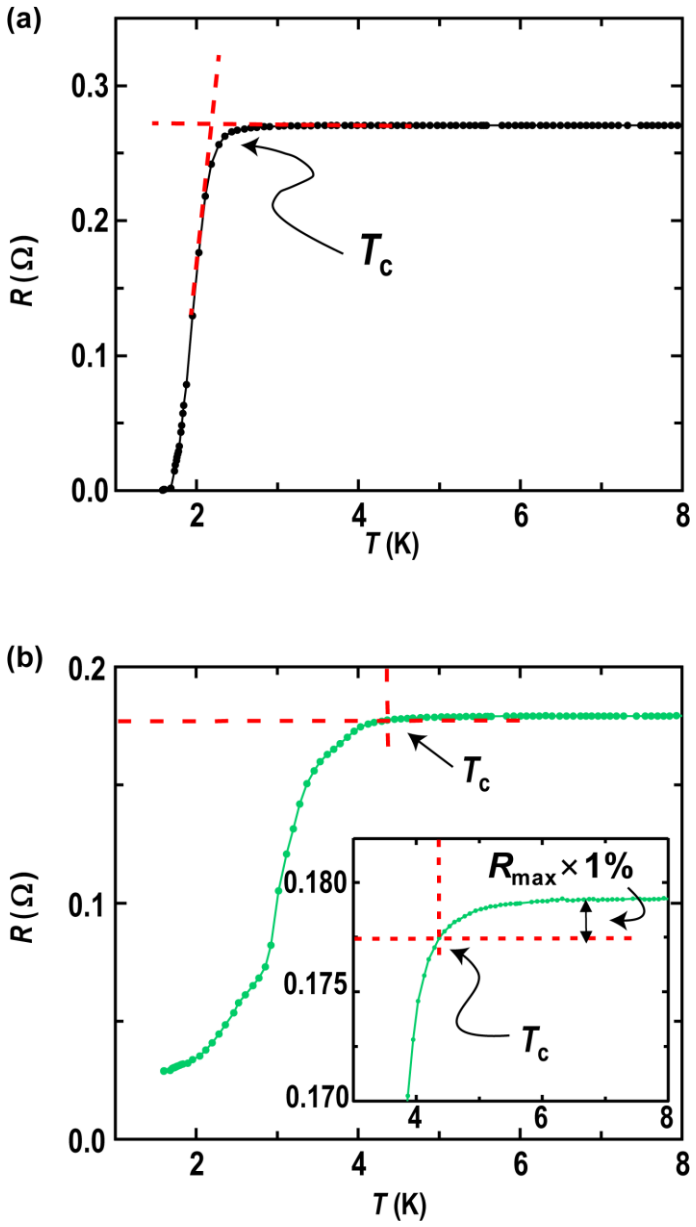

Figure S9. How to determine the T_c values (a) for T_c – p plots (Figure 6(b)) and (b) for h^* - t plots ($t = T/T_c$) (Figures 7(b) and (d)) are shown.

h^* - t plots of $Bi_{2-x}Sb_xTe_{3-y}Se_y$ (x = 0.5, y = 1.0)

The h^* - t plots of $Bi_{1.50(3)}Sb_{0.50(3)}Te_{1.68(6)}Se_{1.32(6)}$ ($Bi_{2-x}Sb_xTe_{3-y}Se_y$ (x = 0.5)) at 8.74, 11.8 and 14.2 GPa were recorded (not shown), indicating that *p*-wave polar model is probably applicable for h^* - t plots at 11.8 and 14.2 GPa; it was unclear if the *p*-wave polar mode is valid for h^* - t plot at 8.74 GPa because of insufficient data. Namely, topological nature may be present in the superconductivity. The h^* - t plots of $Bi_{1.089(8)}Sb_{0.911(8)}Te_{1.81(3)}Se_{1.19(3)}$ ($Bi_{2-x}Sb_xTe_{3-y}Se_y$ (x= 1.0)) were recorded at 8.47 and 11.2 GPa, but it was unclear if the *p*-wave polar mode is applicable for the h^* - t plots because of insufficient data. Also the h^* - t plot has not been recorded for $Bi_{2.1(1)}Te_{1.8(2)}Se_{1.2(2)}$ ($Bi_{2-x}Sb_xTe_{3-y}Se_y$ (x= 0)). However, it is presumed from the analogy of electronic/crystal structures among $Bi_{2-x}Sb_xTe_{3-y}Se_y$ (x = 0, 0.25, 0.5, 1.0; y = 1.0) that these samples' superconductivity may also accompany the topological nature. To sum up, the topological superconductivity is suggested, but it is noticed that the data points are still insufficient to conclude the topological nature in superconductivity.

Theoretical approach for $Bi_{2-x}Sb_xTe_{3-y}Se_y$ (x = 0 and y = 1.0)

Theoretical approach for $Bi_{2-x}Sb_xTe_{3-y}Se_y$ (x = 0 and y = 1.0), Bi_2Te_2Se, was tried to investigate topological nature under pressure. The electronic structure calculations were achieved using the all electron full potential local orbital (FPLO) method [51] and generalized gradient approximation (GGA) exchange and correlation functional [52]. We converge the calculations using 12x12x12 k meshes. For the determination of electronic structures and topological invariants, fully relativistic GGA calculations (GGA+SO) were employed. The band dispersions and DOS are depicted in Figures S10 – S12.

The Z_2 invariant calculated for each crystal phase of Bi_2Te_2Se under pressure indicated a strong topological nature (1;(000)) for phase-I, a topologically trivial nature (0;(000)) for phase-II, and a strong topological nature (1;(001)) for phase-III. Here, it should be noticed that the Z_2 invariant for phase-II is very sensitive to crystal structure, and that the topologically trivial nature is still under discussion. The topological superconductivity suggested from h^*- t plots may be reasonable for phase-I considering the bulk superconductivity and topologically non-trivial electronic structures, although the topological superconductivity is not directly evidenced.

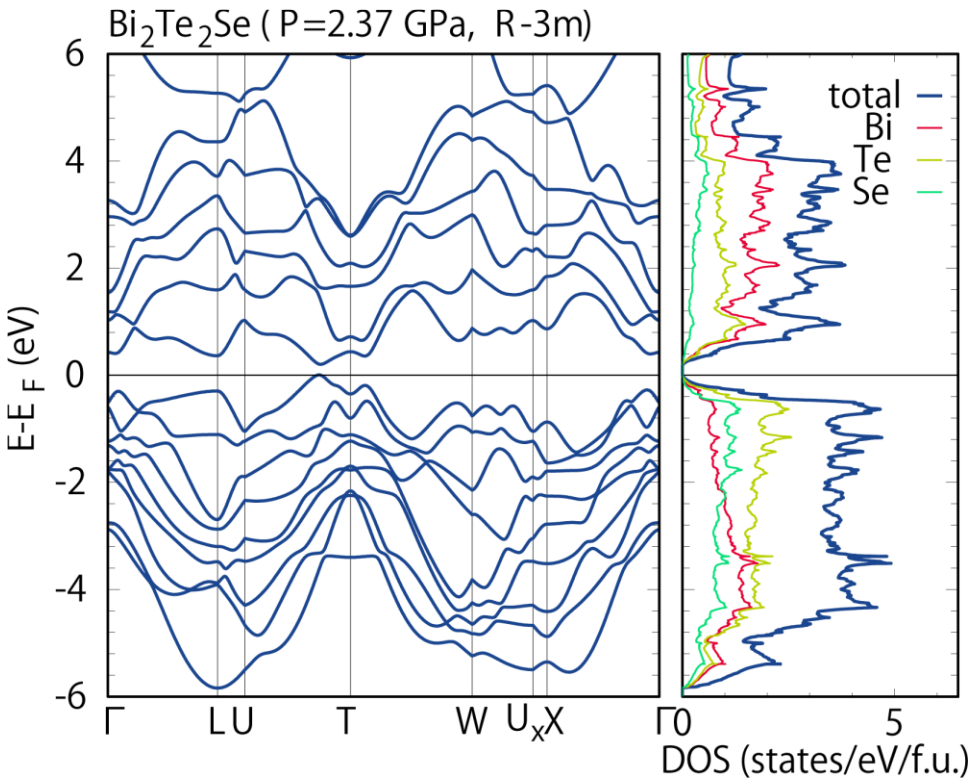

Figure S10. GGA+SO band structure, and DOS of Bi_2Te_2Se at 2.37 GPa.

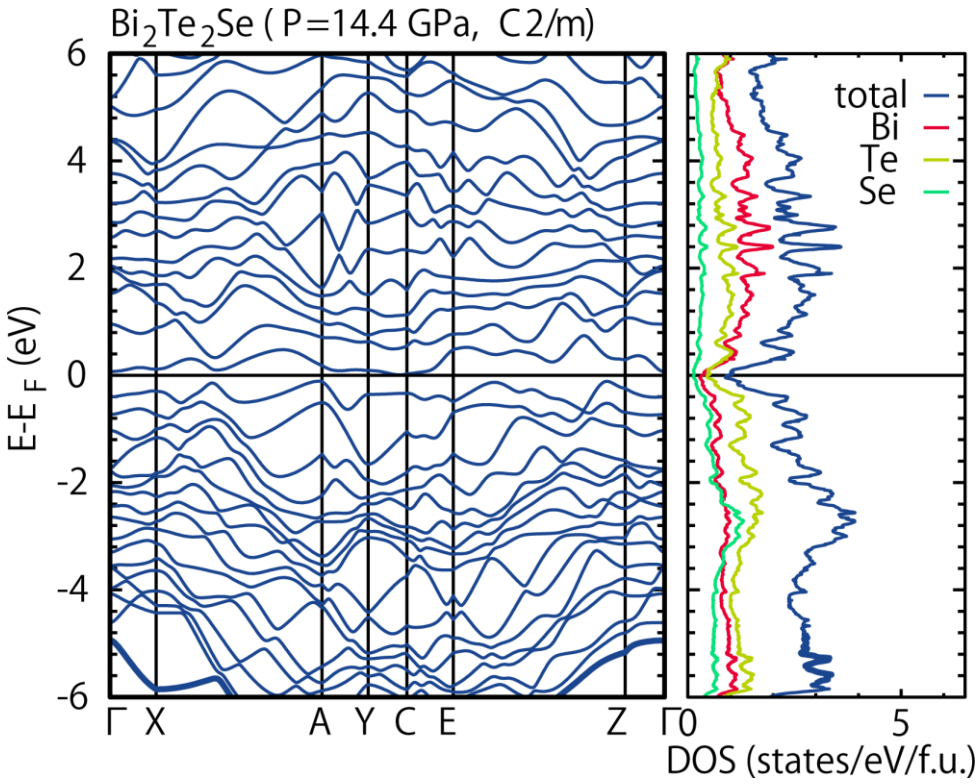

Figure S11. GGA+SO band structure, and DOS of Bi_2Te_2Se at 14.4 GPa.

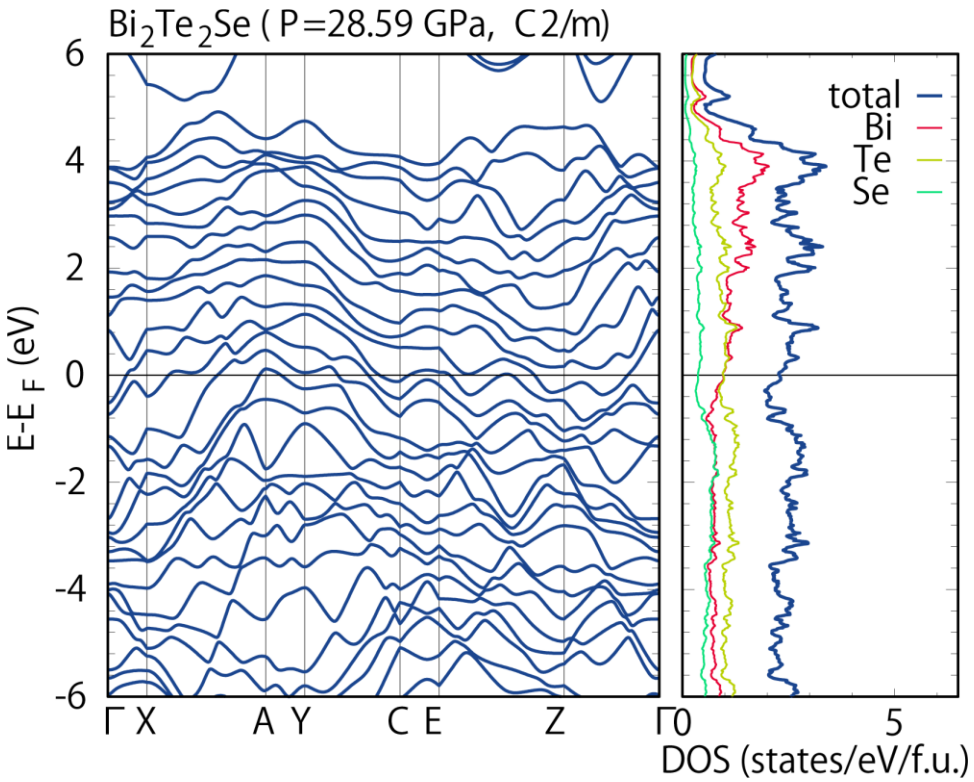

Figure S12. GGA+SO band structure, and DOS of Bi_2Te_2Se at 28.6 GPa.

Table S1. Atomic coordinates of $Bi_{2-x}Sb_xTe_{3-y}Se_y$. Nominal stoichiometry is shown as follows (see Table 1 for the stoichiometry determined from the EDX).

Bi_2Te_2Se: Rhombohedral ($R\bar{3}m$; No. 166)

Atom	Site	Occupancy	x	y	z	*B* (Å²)
Bi	6c	1	0.00000	0.00000	0.39603(4)	1.19(4)
Te	6c	0.73(3)	0.00000	0.00000	0.21212(8)	1.09(6)
Se1	6c	0.27(3)	0.00000	0.00000	0.21212(8)	1.09(6)
Se2	3a	1	0.00000	0.00000	0.00000	0.59(7)

$Bi_{1.75}Sb_{0.25}Te_2Se$: Rhombohedral ($R\bar{3}m$; No. 166)

Atom	Site	Occupancy	x	y	z	*B* (Å²)
Bi	6c	0.84(4)	0.00000	0.00000	0.39557(4)	1.04(4)
Sb	6c	0.16(4)	0.00000	0.00000	0.39557(4)	1.04(4)
Te	6c	0.82(4)	0.00000	0.00000	0.21254(8)	0.96(7)
Se1	6c	0.18(4)	0.00000	0.00000	0.21254(8)	0.96(7)
Se2	3a	1	0.00000	0.00000	0.00000	0.56(12)

$Bi_{1.5}Sb_{0.5}Te_2Se$: Rhombohedral ($R\bar{3}m$; No. 166)

Atom	Site	Occupancy	x	y	z	*B* (Å²)
Bi	6c	0.79(2)	0.00000	0.00000	0.39543(6)	1.03(7)
Sb	6c	0.21(2)	0.00000	0.00000	0.39543(6)	1.03(7)
Te	6c	1	0.00000	0.00000	0.21308(9)	1.01(8)
Se	3a	1	0.00000	0.00000	0.00000	0.13(8)

$BiSbTe_2Se$: Rhombohedral ($R\bar{3}m$; No. 166)

Atom	Site	Occupancy	x	y	z	*B* (Å²)
Bi	6c	0.55(8)	0.00000	0.00000	0.39509(6)	0.99(5)
Sb	6c	0.45(8)	0.00000	0.00000	0.39509(6)	0.99(5)
Te1	6c	0.85(11)	0.00000	0.00000	0.21352(8)	0.97(7)
Te2	3a	0.10(8)	0.00000	0.00000	0.00000	0.62(11)
Se1	6c	0.15(11)	0.00000	0.00000	0.21352(8)	0.97(7)
Se2	3a	0.90(8)	0.00000	0.00000	0.00000	0.62(11)

Table S2. Atomic coordinates of Bi_2Te_2Se and lattice constants for each phase determined by Rietveld refinement: Nominal stoichiometry is shown as follows (see Table 1 for the stoichiometry determined from the EDX).

Bi_2Te_2Se: Rhombohedral ($R\bar{3}m$; No. 166) (phase-I, 2.37 GPa)

Atom	Site	Occupancy	x	y	z	*B* (Å^2)
Bi	6c	0.8712	0.000000	0.000000	0.396716	0.78
Te	6c	0.9416	0.000000	0.000000	0.209730	1.44
Se	3a	1.1556	0.000000	0.000000	0.000000	7.07

Bi_2Te_2Se: Monoclinic (*C*2/m; No. 12) (phase-II, 14.4 GPa)

Atom	Site	Occupancy	x	y	z	*B* (Å^2)
Bi1	4i	1.0059	0.180679	0.000000	0.199947	2.57
Bi2	4i	0.7437	0.399535	0.000000	0.171052	1.00
Te1	4i	1.1294	0.208266	0.000000	0.389514	0.70
Te2	4i	1.0274	0.058301	0.000000	-0.363962	1.07
Se	4i	1.1646	0.369983	0.000000	0.002593	2.30

Bi_2Te_2Se: Monoclinic (*C*2/m; No. 12) (phase-III, 28.6 GPa)

Atom	Site	Occupancy	x	y	z	*B* (Å^2)
Bi1	4i	0.5872	0.407391	0.000000	-0.371507	1.30
Bi2	4i	0.6691	0.195807	0.000000	-0.180444	1.83
Te1	4i	1.0053	-0.200894	0.000000	-0.321039	1.73
Te2	2c	0.9041	0.000000	0.000000	-0.500000	2.06
Te3	2a	0.8252	0.000000	0.000000	0.000000	1.08
Se	4i	1.3783	0.401861	0.000000	0.075310	0.53

Lattice constants for three phases in Bi_2Te_2Se

Pressure (GPa)	phase	Space group	*a* (Å)	*b* (Å)	*c* (Å)	β
2.37	I	$R\bar{3}m$	4.2103(1)	-	29.130(2)	-
14.4	II	*C*2/m	14.1147(8)	3.9425(3)	16.894(1)	148.856°
28.6	III	*C*2/m	14.854(2)	4.8906(3)	6.0947(9)	105.532°